Physica D 239 (2010) 1958–1967

Contents lists available at ScienceDirect

Physica D

journal homepage: www.elsevier.com/locate/physd

Filtering and frequency interpretations of Singular Spectrum Analysis

T.J. Harris *, Hui Yuan

Department of Chemical Engineering, Queen's University, Kingston, ON, K7L 3N6, Canada

ARTICLE INFO

Article history:
Received 26 June 2009
Received in revised form
21 May 2010
Accepted 21 July 2010
Available online 25 July 2010
Communicated by J. Bronski

Keywords:
Singular Spectrum Analysis
Toeplitz matrix
Persymmetric matrix
Eigenfilter
Convolution filter
Zero-phase filter

ABSTRACT

New filtering and spectral interpretations of Singular Spectrum Analysis (SSA) are provided. It is shown that the variables reconstructed from diagonal averaging of reduced-rank approximations to the trajectory matrix can be obtained from a noncausal convolution filter with zero-phase characteristics. The reconstructed variables are readily constructed using a two-pass filtering algorithm that is well known in the signal processing literature. When the number of rows in the trajectory matrix is much larger than number of columns, many results reported in the signal processing literature can be used to derive the properties of the resulting filters and their spectra. New features of the reconstructed series are revealed using these results. Two examples are used to illustrate the results derived in this paper.

1. Introduction

Singular Spectrum Analysis (SSA) has proven to be a flexible method for the analysis of time-series data. Applications are reported in diverse areas such as climate change and geophysical phenomena [1–3], mineral processing [4] and telecommunication applications [5,6]. The basic SSA method has been combined with the maximum entropy method (MEM) [7] and with multi-taper methods [8] to enhance the spectral analysis of data. Extensions to cope with missing data [9] and multi-scale applications have also been developed [10].

The basic elements of SSA were first reported in [11,12]. Widespread use of SSA followed a series of papers by Vautard and Ghil [2] and Vautard et al. [3]. The monograph by Golyandina et al. [13] describes the basic algorithm plus a number of variations. A recent overview is given in [14].

The purpose of this paper is to give a number of interpretations of SSA from a signal processing perspective by addressing issues related to filtering interpretations, spectrum evaluation and recovery of harmonic signals. In particular, in the case where the trajectory matrix has many more rows than columns, the eigenvalues and eigenvectors are nearly identical to those of an associated symmetric Toeplitz matrix. The eigenvalues and eigenvectors of this latter matrix are highly structured [15–17]. These structured properties lead to a number of interesting filtering interpretations. Additionally, we note that the reconstruction phase in SSA can be interpreted as a forward and a reverse filtering of the original data. This provides for a number of additional interpretations for the filtered series and their spectra.

The paper is organized as follows. In the next section we state the basic SSA algorithm and some variations. This is followed by filtering and spectral interpretations of the SSA algorithm. These interpretations make extensive use of symmetry properties of the eigenfilters that are used in the filtering. These in turn are derived from symmetry properties of the eigenvectors of the trajectory matrix. Two examples are then analyzed to illustrate the theoretical results.

2. Basic SSA and some variations

2.1. Basic SSA algorithm

The basic SSA algorithm consists of the following steps [2,3,12].

1. Choose an embedded dimension K and define $L = N + 1 - K$, where N is the number of observations in the time series.
2. Form the $L \times K$ Hankel matrix $\boldsymbol{A}$ using mean-corrected data, $y_t,\ t = 1, 2, \ldots, N$.

$$\boldsymbol{A} = [\boldsymbol{y}_1, \boldsymbol{y}_2, \boldsymbol{y}_3, \ldots, \boldsymbol{y}_K] = \begin{bmatrix} y_1 & y_2 & y_3 & \cdots & \cdots & y_K \\ y_2 & y_3 & y_4 & \cdots & \cdots & y_{K+1} \\ y_3 & y_4 & y_5 & \cdots & \cdots & y_{K+2} \\ \vdots & \vdots & \vdots & & & \vdots \\ y_L & y_{L+1} & y_{L+2} & \cdots & \cdots & y_{K+L-1} \end{bmatrix}$$

* Corresponding author. Tel.: +1 613 533 2765.
E-mail address: tom.harris@chee.queensu.ca (T.J. Harris).
URL: http://chemeng.queensu.ca/people/faculty/harris (T.J. Harris).

0167-2789/$ – see front matter © 2010 Elsevier B.V. All rights reserved.
doi:10.1016/j.physd.2010.07.005

where $\boldsymbol{y}_i = (y_i, y_{i+1}, \ldots, y_{i+L-1})^T$. This matrix $\boldsymbol{A}$ is often referred to as the trajectory matrix. In most applications of SSA, $L > K$ [2,13].

3. Determine the eigenvalues and eigenvectors of $\boldsymbol{A}^T\boldsymbol{A}$. Denote the eigenvalues by $\lambda_1 \geq \lambda_2 \geq \cdots \geq \lambda_K \geq 0$. For each eigenvalue λ_i there is a corresponding eigenvector $\boldsymbol{v}_i$.

$$(\boldsymbol{A}^T\boldsymbol{A})\boldsymbol{v}_i = \lambda_i \boldsymbol{v}_i. \tag{1}$$

4. Define K new series, $\boldsymbol{w}_i = \boldsymbol{A}\boldsymbol{v}_i$, $i = 1, 2, \ldots, K$. Each series is of length L. Once the new series are constructed, the analysis then focuses on the new series, which are sometimes referred to as the latent variables. The individual series may be analyzed, or subsets may be grouped together.

   The utility of the method is derived from the following properties and interpretations of the eigenvalue analysis:

   (a) The eigenvectors $\boldsymbol{v}_i$ are orthonormal, i.e., $\boldsymbol{v}_i^T\boldsymbol{v}_j = 0$ $(i \neq j)$ and $\boldsymbol{v}_i^T\boldsymbol{v}_i = 1$.

   (b) The latent variables $\boldsymbol{w}_i$ are orthogonal, and
   $$\|\boldsymbol{w}_i\|^2 = \boldsymbol{w}_i^T\boldsymbol{w}_i = (\boldsymbol{A}\boldsymbol{v}_i)^T\boldsymbol{A}\boldsymbol{v}_i = \boldsymbol{v}_i^T(\boldsymbol{A}^T\boldsymbol{A})\boldsymbol{v}_i$$
   $$= \boldsymbol{v}_i^T\lambda_i\boldsymbol{v}_i = \lambda_i. \tag{2}$$

   (c) Consequently,
   $$\sum_{i=1}^{K}\boldsymbol{w}_i^T\boldsymbol{w}_i = \sum_{i=1}^{K}\boldsymbol{w}_i^T\sum_{i=1}^{K}\boldsymbol{w}_i = \sum_{i=1}^{K}\lambda_i. \tag{3}$$

Often, the interesting features of a time series are found by analyzing the first few latent variables. A number of methods have been proposed to choose the number of latent variables for analysis. Most often, the construction of a scree plot [18], which is a plot of λ_i versus i, will indicate a knee or bend. This can be used to select the number of latent variables. Other methods have been proposed when the break points are not clear [19].

Scree plots are also useful for identifying harmonics in the data. As discussed in [2,12,14], if N and L are large enough, each harmonic results in two eigenvalues that are closely paired for a purely harmonic series. A harmonic component may produce a periodic component in the autocorrelation and partial autocorrelation function. However, the number of periodic components cannot be easily extracted from these functions. In addition, a slowly decreasing sequence of eigenvalues can be produced by a pure noise series [13,14]. These two observations suggest that a break or knee in the scree plot can be used to separate the signals that arise from harmonics and signals from noise or aperiodic components [13].

The eigenvalues of $\boldsymbol{A}^T\boldsymbol{A}$ are most often calculated by undertaking a singular value decomposition (SVD) of $\boldsymbol{A}$. The right singular vectors of $\boldsymbol{A}$ are identical with the eigenvectors of $\boldsymbol{A}^T\boldsymbol{A}$ and the eigenvalues of this latter matrix are the squares of the corresponding singular values of $\boldsymbol{A}$ [13].

2.2. Variation: Toeplitz approximation to $\boldsymbol{A}^T\boldsymbol{A}$

$\boldsymbol{A}^T\boldsymbol{A}$ is symmetric and positive semi-definite. It can be written as

$$\boldsymbol{A}^T\boldsymbol{A} = \begin{bmatrix} \boldsymbol{y}_1^T\boldsymbol{y}_1 & \boldsymbol{y}_1^T\boldsymbol{y}_2 & \cdots & \boldsymbol{y}_1^T\boldsymbol{y}_K \\ \boldsymbol{y}_2^T\boldsymbol{y}_1 & \boldsymbol{y}_2^T\boldsymbol{y}_2 & \cdots & \boldsymbol{y}_2^T\boldsymbol{y}_K \\ \vdots & \vdots & & \vdots \\ \boldsymbol{y}_K^T\boldsymbol{y}_1 & \boldsymbol{y}_K^T\boldsymbol{y}_2 & \cdots & \boldsymbol{y}_K^T\boldsymbol{y}_K \end{bmatrix}.$$

In situations when $L \gg K$, we have

$$\frac{1}{L}\boldsymbol{y}_1^T\boldsymbol{y}_1 \simeq \frac{1}{L}\boldsymbol{y}_2^T\boldsymbol{y}_2 \simeq \frac{1}{L}\boldsymbol{y}_3^T\boldsymbol{y}_3 \simeq \cdots \simeq \frac{1}{L}\boldsymbol{y}_K^T\boldsymbol{y}_K \simeq \frac{1}{N}\sum_{t=1}^{N} y_t^2 = c_0$$

$$\frac{1}{L}\boldsymbol{y}_1^T\boldsymbol{y}_2 \simeq \frac{1}{L}\boldsymbol{y}_2^T\boldsymbol{y}_3 \simeq \cdots \simeq \frac{1}{L}\boldsymbol{y}_{K-1}^T\boldsymbol{y}_K \simeq \frac{1}{N-1}\sum_{t=1}^{N-1} y_t y_{t-1} = c_1$$

$$\vdots$$

$$\frac{1}{L}\boldsymbol{y}_1^T\boldsymbol{y}_K = \frac{1}{L}\sum_{t=1}^{L} y_t y_{t-(K-1)} = c_{K-1}$$

where c_i is the sample autocovariance at lag i (we have previously assumed that the data have been mean corrected). Consequently

$$\frac{\boldsymbol{A}^T\boldsymbol{A}}{L} \simeq \boldsymbol{C} = \begin{bmatrix} c_0 & c_1 & \cdots & c_{K-1} \\ c_1 & c_0 & \cdots & c_{K-2} \\ \vdots & \vdots & & \vdots \\ c_{K-1} & c_{K-2} & \cdots & c_0 \end{bmatrix}$$

where $\boldsymbol{C}$ is the sample covariance matrix of the observations. The sample autocorrelation matrix $\boldsymbol{R} = \boldsymbol{C}/c_0$ is often used instead of $\boldsymbol{C}$ for analysis. This is appropriate when the data have been centered and normalized [12,20].

2.3. Variation: Hankel approximation and diagonal averaging [13]

A singular value decomposition of the matrix is undertaken

$$\boldsymbol{A} = \sum_{i=1}^{\mu}\boldsymbol{X}_i = \sum_{i=1}^{\mu}\sqrt{\lambda_i}\boldsymbol{u}_i\boldsymbol{v}_i^T \tag{4}$$

where $\mu = \min(L, K)$, λ_i and $\boldsymbol{v}_i$ are the eigenvalues and eigenvectors of $\boldsymbol{A}^T\boldsymbol{A}$ as described in Eq. (1), and $\boldsymbol{u}_i$ are the eigenvectors of $\boldsymbol{A}\boldsymbol{A}^T$, i.e., the solution to [21]

$$(\boldsymbol{A}\boldsymbol{A}^T)\boldsymbol{u}_i = \lambda_i\boldsymbol{u}_i. \tag{5}$$

The orthogonal vectors $\boldsymbol{u}_i$ and $\boldsymbol{v}_i$ are related by

$$\boldsymbol{A}\boldsymbol{v}_i = \sqrt{\lambda_i}\boldsymbol{u}_i, \quad i = 1, 2, \ldots, \mu \tag{6}$$

where the singular values of $\boldsymbol{A}$ are $\sqrt{\lambda_i}$, i.e., the square root of the eigenvalues of $\boldsymbol{A}^T\boldsymbol{A}$. Clearly, $\boldsymbol{u}_i = \boldsymbol{w}_i/\sqrt{\lambda_i}$.

Each of the $\boldsymbol{X}_i$ in Eq. (4) is of rank 1. A new series $\boldsymbol{x}_i$ of length N is reconstructed by averaging each of the N anti-diagonals in $\boldsymbol{X}_i$. Attention is then focused on the new series $\boldsymbol{x}_i$, or groupings of these series. Guidelines for grouping of variables are typically based on the clustering and separation of the eigenvalues. A 'separability index' has been proposed in [14] to assist with grouping.

This diagonal averaging is computationally equivalent to calculating $\boldsymbol{x}_i$ using [22]

$$\boldsymbol{x}_i = \boldsymbol{D}^{-1}\boldsymbol{W}_i\boldsymbol{v}_i \tag{7}$$

where

$$\boldsymbol{W}_i = \begin{pmatrix} w_1 & 0 & \cdots & \cdots & \cdots & 0 \\ w_2 & w_1 & 0 & \cdots & \cdots & 0 \\ w_3 & w_2 & w_1 & 0 & \cdots & 0 \\ \vdots & & \vdots & \vdots & & \vdots \\ w_{K-1} & \cdots & w_3 & w_2 & w_1 & 0 \\ w_K & \cdots & \cdots & w_3 & w_2 & w_1 \\ w_{K+1} & \cdots & \cdots & \cdots & w_3 & w_2 \\ \vdots & & & & & \vdots \\ w_{L-1} & w_{L-2} & \cdots & \cdots & \cdots & w_{L-K} \\ w_L & w_{L-1} & w_{L-2} & \cdots & \cdots & w_{L-K+1} \\ 0 & w_L & w_{L-1} & w_{L-2} & \cdots & w_{L-K+2} \\ \vdots & & \vdots & \vdots & & \vdots \\ 0 & \cdots & 0 & w_L & w_{L-1} & w_{L-2} \\ 0 & \cdots & \cdots & 0 & w_L & w_{L-1} \\ 0 & \cdots & \cdots & \cdots & 0 & w_L \end{pmatrix} \tag{8}$$

and $\boldsymbol{D}$ is an $N \times N$ diagonal matrix, whose diagonal elements are

$$\begin{pmatrix} 1 & 2 & \cdots & \mu-1 & \mu & \cdots & \mu & \mu-1 & \cdots & 2 & 1 \end{pmatrix} \tag{9}$$

and $\boldsymbol{w}_i = \begin{pmatrix} w_1 & w_2 & \cdots & w_L \end{pmatrix}^T = \boldsymbol{A}\boldsymbol{v}_i$, and $\boldsymbol{v}_i$ is one of the eigenvectors. To simplify the nomenclature, double subscripting on $\boldsymbol{w}_i$ has been avoided. It is understood that the elements of this vector depend upon the specific eigenvector used in the reconstruction.

Recall that $N = L + K - 1$ and $\mu = min(L, K) = K$ in most SSA applications. Then there are $N - 2(K-1) = 2L - N$ 'complete' rows with diagonal elements μ in $\boldsymbol{D}$. The matrix $\boldsymbol{W}_i$ is of dimension $N \times K$. The first and last $K-1$ rows are 'incomplete', which leaves $N - 2(K-1)$ 'complete' rows.

The latent variables $\boldsymbol{w}_i$ are orthogonal, and have squared norm $\|\boldsymbol{w}_i\|_2^2 = \lambda_i$. The squared norm of a reconstructed series using diagonal averaging is

$$\begin{aligned} \|\boldsymbol{x}_i\|_2^2 &= \|\boldsymbol{D}^{-1}\boldsymbol{W}_i\boldsymbol{v}_i\|_2^2 \\ &\le \|\boldsymbol{D}^{-1}\|_2^2 \cdot \mathrm{trace}(\boldsymbol{W}_i^T\boldsymbol{W}_i) \\ &= K\|\boldsymbol{D}^{-1}\|_2^2 \cdot \|\boldsymbol{w}_i\|_2^2 \\ &= K\lambda_i\|\boldsymbol{D}^{-1}\|_2^2 \\ &= \frac{K\lambda_i}{2(1+1/4+1/9+\cdots 1/(K-1)^2)+(2L-N)/K^2} \\ &\simeq \frac{K}{\pi^2/3+(2L-N)/K^2}\lambda_i, \quad L \gg K \end{aligned} \tag{10}$$

and

$$\left\| \sum_{i=1}^{d} \boldsymbol{x}_i \right\|_2^2 \neq \sum_{i=1}^{d} \|\boldsymbol{x}_i\|_2^2. \tag{11}$$

Calculations indicate that the upper bound may be quite conservative. The reconstructed series $\boldsymbol{x}_i$ are not orthogonal making it impossible to calculate the variance of grouped variables from the variance of the individual reconstructed series.

The use of reduced-rank approximations to assist in the extraction of harmonic signals from additive noise has been considered extensively in the signal processing literature [23–25]. The trajectory matrix has a central role in these algorithms. Extensive research indicates that extraction of these signals is considerably enhanced when the trajectory matrix is replaced by a structured low-rank approximation [26,27]. The SVD leads to an unstructured approximation, because the $\boldsymbol{X}_i$ are not Hankel. A structured approximation is obtained when the trajectory matrix is calculated using the reconstructed series (or groupings of variables). While the SVD does not preserve the Hankel structure, the Hankel matrix constructed from the reconstructed series does not preserve the rank property. Cadzow [28] developed a simple iterative algorithm to preserve both the rank and Hankel structure. He has shown that this iteration will converge to reduced-rank approximation that has the Hankel structure for certain classes of signals including sinusoids and damped sinusoids corrupted by white noise. The reconstruction of the $\boldsymbol{x}_i$ corresponds to one iteration of Cadzow's algorithm. Other approaches for obtaining reduced-rank approximations with appropriate structure involve the use of structured total least squares [29–31]. These methods are computationally intense, requiring the use of a nonlinear optimizer in high dimension.

3. Filtering interpretation of SSA

Before discussing filtering interpretations, we state a number of definitions and properties.

Definition 1. A column vector $\boldsymbol{c}$ of length n is symmetric if $\boldsymbol{c}$ equals the vector obtained by reversing the rows of $\boldsymbol{c}$, i.e., $c_i = c_{n+1-i}$, $i = 1, 2, \ldots, n$. Mathematically, $\boldsymbol{c}$ is symmetric, if $\boldsymbol{J}\boldsymbol{c} = \boldsymbol{c}$, where $\boldsymbol{J}$ is a $n \times n$ matrix with ones on the main anti-diagonal. $\boldsymbol{J}$ is known as the exchange matrix.

A vector $\boldsymbol{c}$ is skew-symmetric if the vector obtained by reversing the rows of $\boldsymbol{c}$ equals $-\boldsymbol{c}$, i.e., $c_i = -c_{n+1-i}$, $i = 1, 2, \ldots, n$. A skew-symmetric vector satisfies $\boldsymbol{J}\boldsymbol{c} = -\boldsymbol{c}$.

Table 1
Eigenvector patterns for persymmetric matrices. $\boldsymbol{J}$ is the $[K/2] \times [K/2]$ exchange matrix.

K	Symmetric eigenvector	Skew-symmetric eigenvector
Odd	$\begin{pmatrix} \boldsymbol{\alpha}_i^T\boldsymbol{J} & \alpha_0 & \boldsymbol{\alpha}_i^T \end{pmatrix}^T$	$\begin{pmatrix} -\boldsymbol{\beta}_i^T\boldsymbol{J} & 0 & \boldsymbol{\beta}_i^T \end{pmatrix}^T$
Even	$\begin{pmatrix} \boldsymbol{\alpha}_i^T\boldsymbol{J} & \boldsymbol{\alpha}_i^T \end{pmatrix}^T$	$\begin{pmatrix} -\boldsymbol{\beta}_i^T\boldsymbol{J} & \boldsymbol{\beta}_i^T \end{pmatrix}^T$

Definition 2. An $n \times n$ matrix $\boldsymbol{X}$ is persymmetric if it is symmetric about both its main diagonal and main anti-diagonal. A symmetric Toeplitz matrix is persymmetric.

Property 1. *If a persymmetric matrix has K distinct eigenvalues, then there are $[(K+1)/2]$ symmetric eigenvectors, and $[K/2]$ skew-symmetric eigenvectors, where $[x]$ denotes the integer part of x [15–17]. The eigenvectors appear in the pattern shown in Table 1.*

Property 2. *The eigenvectors of a persymmetric matrix $\boldsymbol{X}$ can be computed from matrices of lower dimension [15,16]. For K even, $\boldsymbol{X}$ can be written as*

$$\boldsymbol{X} = \begin{pmatrix} \boldsymbol{X}_{11} & \boldsymbol{J}\boldsymbol{X}_{21}\boldsymbol{J} \\ \boldsymbol{X}_{21} & \boldsymbol{J}\boldsymbol{X}_{11}\boldsymbol{J} \end{pmatrix} \tag{12}$$

where $\boldsymbol{X}_{11}$ and $\boldsymbol{X}_{21}$ are $[K/2] \times [K/2]$ and $\boldsymbol{X}_{11}^T = \boldsymbol{X}_{11}$, $\boldsymbol{X}_{21}^T = \boldsymbol{J}\boldsymbol{X}_{21}\boldsymbol{J}$. $[K/2]$ eigenvalues p_i, and associated symmetric eigenvectors $\tilde{\boldsymbol{\alpha}}_i$, are obtained from the eigenvalue problem

$$(\boldsymbol{X}_{11} + \boldsymbol{J}\boldsymbol{X}_{21})\tilde{\boldsymbol{\alpha}}_i = p_i\tilde{\boldsymbol{\alpha}}_i \tag{13}$$

$\boldsymbol{\alpha}_i$ in Table 1 is given by $\boldsymbol{\alpha}_i = \frac{1}{\sqrt{2}}\tilde{\boldsymbol{\alpha}}_i$ and $i = 1, 2, \ldots, [K/2]$.

The remaining $[K/2]$ skew-symmetric eigenvectors $\tilde{\boldsymbol{\beta}}_i$, and corresponding eigenvalues q_i, are determined from the eigenvalue problem

$$(\boldsymbol{X}_{11} - \boldsymbol{J}\boldsymbol{X}_{21})\tilde{\boldsymbol{\beta}}_i = q_i\tilde{\boldsymbol{\beta}}_i \tag{14}$$

$\boldsymbol{\beta}_i$ in Table 1 is obtained from $\boldsymbol{\beta}_i = \frac{1}{\sqrt{2}}\tilde{\boldsymbol{\beta}}_i$ and again $i = 1, 2, \ldots, [K/2]$.

The eigenvectors have considerable structures. This structure will be exploited in Section 3.2. Expressions for K odd can be found in [15].

Definition 3. Let $b(x)$ be a polynomial of the form $b(x) = \sum_{k=1}^{n} b_k x^{k-1}$. $b(x)$ is a palindromic polynomial if $b_k = b_{n-k+1}$, $k = 1, 2, \ldots, n$. $b(x)$ is an antipalindromic polynomial if $b_k = -b_{n-k+1}$, $k = 1, 2, \ldots, n$ [32].

Definition 4. For a polynomial $b(x)$ with real coefficients, the reciprocal polynomial of $b(x) = \sum_{k=1}^{n} b_k x^{k-1}$ is obtained by reversing the coefficients, i.e., $\tilde{b}(x) = \sum_{k=1}^{n} b_{n-k+1} x^{k-1}$.

Definition 5. An eigenfilter is a polynomial formed filter whose polynomial coefficients are obtained from an eigenvector. Denoting an eigenvector by $\boldsymbol{v}$ the associated eigenfilter is $v(z^{-1}) = \sum_{k=1}^{K} v_k z^{-(k-1)}$, where z^{-1} is interpreted as the backshift operator, i.e., $z^{-1}y_t = y_{t-1}$.

Property 3. *The eigenfilters constructed from a persymmetric matrix are either palindromic polynomials or antipalindromic polynomials. This follows immediately from the symmetric and skew-symmetric properties of the eigenvectors of symmetric Toeplitz matrices (Property 2).*

Table 2
Distribution of roots at $z = \pm 1$ for eigenfilters of a symmetric Toeplitz matrix.

Type	Order $(K-1)$	Root at $z^{-1}=1$	Root at $z^{-1}=-1$
Antipalindrome	Odd	✓	–
	Even	✓	✓
Palindrome	Odd	–	✓
	Even	–	–

Property 4. *The roots of the eigenfilters constructed from a persymmetric matrix have unit magnitude, or they appear in reciprocal pairs* [17,32].

Property 5. *The distribution of roots at $z = \pm 1$ of the eigenfilters constructed from a symmetric Toeplitz matrix is given in Table 2. These results are established by substituting $z = \pm 1$ into those palindromic and antipalindromic polynomials. It is known that an antipalindromic polynomial always has an odd number of roots located at $z^{-1} = 1$* [32].

Property 6. *When the eigenvalues of a symmetric Toeplitz matrix are unique, the roots of the eigenfilter associated with the minimum/maximum eigenvalue all lie on the unit circle. For the other eigenfilters, this property may or may not be satisfied* [17,33,34].

3.1. Filtering interpretation of latent variables

The latent variable $\boldsymbol{w}_i$ is readily interpreted as a filtered value of the original variables. To simplify the notation, let $\boldsymbol{v}$ be one of the eigenvectors and $\boldsymbol{w}$ be the corresponding filtered value instead of $\boldsymbol{v}_i$ and $\boldsymbol{w}_i$. Then, the tth element of $\boldsymbol{w}$ can be written as

$$w_t = \sum_{m=1}^{K} v_m y_{t+m-1}, \quad t = 1, 2, \ldots, L. \tag{15}$$

Alternatively, it can be written in the form

$$w_t = \sum_{m=1}^{K} \tilde{v}_m y_{t+K-m}, \quad t = 1, 2, \ldots, L$$

where the coefficients $\tilde{v}_m$ are obtained by simply reversing the order of the coefficients v_m. This can be expressed mathematically as $\tilde{\boldsymbol{v}} = \boldsymbol{J}\boldsymbol{v}$, where $\boldsymbol{J}$ is again a $K \times K$ exchange matrix (Definition 1).

3.2. Filtering interpretations using the Toeplitz approximation

Let the eigenvectors be obtained from the Toeplitz approximation to $\boldsymbol{A}^T\boldsymbol{A}$, i.e., $L\boldsymbol{C}$. Based on the definitions, the covariance matrix $\boldsymbol{C}$ is a symmetric Toeplitz matrix and is persymmetric. For the moment, let K be odd. From Property 1, the filtered values for the symmetric eigenvectors can be written as

$$w_t = \alpha_0 y_{t+[K/2]} + \sum_{m=1}^{[K/2]} \alpha_m (y_{t+[K/2]+m} + y_{t+[K/2]-m}), \quad t = 1, 2, \ldots, L. \tag{16}$$

The filtered values using the skew-symmetric eigenvectors are calculated as

$$w_t = \sum_{m=1}^{[K/2]} \beta_m (y_{t+[K/2]+m} - y_{t+[K/2]-m}), \quad t = 1, 2, \ldots, L \tag{17}$$

$\boldsymbol{w}$ can be interpreted as an aligned or time-shifted value, which consists of either a weighted average of $[K/2]$ observed values adjacent to $y_{t+[K/2]}$ in the case of a symmetric eigenvector, or as a weighted difference for a skew-symmetric eigenvector. When plotting y_t and w_t, it is imperative to properly align the original data by aligning $y_{t+[K/2]}$ with w_t.

The filters in Eqs. (16) and (17) are recognized as noncausal Finite Impulse Response (FIR) filters, also called noncausal or nonrecursive filters [35,36]. Eq. (16) describes a zero-phase filter. While the filter may attenuate or amplify the data, it introduces no phase shift in the filtered values. If a series is described by purely harmonic components, these will appear at the same time point in the filtered data as in the original data. Eq. (17) describes a differentiating filter. This filter introduces a phase lag of $\pm\pi$ radians. In a series with purely harmonic components, the filtered series will either lead or lag the original series. There are many classical design techniques for zero-phase filters that act as either averaging filters or differentiating filters [36].

The relationship between the even and odd filters can be expanded by using the alternate calculation method for the symmetric and skew-symmetric eigenvectors that follows from Property 2. When $L \gg K$, the symmetric eigenvectors, and corresponding eigenvalues, can be calculated from

$$\boldsymbol{C}_{11} + \boldsymbol{J}\boldsymbol{C}_{21} \simeq \frac{2}{L}\boldsymbol{A}_1^T\boldsymbol{A}_1 \tag{18}$$

where $\boldsymbol{A}_1$ is the $L \times ([K/2]+1)$ matrix (Eq. (19) given in Box I).

The skew-symmetric eigenvectors are obtained by replacing the sum of the variables by their differences in Eq. (19) (see Eq. (20) given in Box II).

For an even K, the similar patterns can be obtained.

3.3. Filtering interpretation of reconstructed series

From Eqs. (7) and (8), we can show that

$$x_t = \frac{1}{K}\left(y_t + \sum_{m=1}^{K-1} \zeta_m (y_{t-m} + y_{t+m})\right), \quad t = K, K+1, \ldots, N-K+1. \tag{21}$$

The filter coefficients are recognized as $\frac{\boldsymbol{v} \circ \tilde{\boldsymbol{v}}}{K}$, where $\circ$ denotes convolution and $\tilde{\boldsymbol{v}}$ is again obtained by reversing the order of the coefficients of $\boldsymbol{v}$.

$$\begin{aligned}
\zeta_1 &= v_1 v_2 + v_2 v_3 + \cdots + v_{K-2} v_{K-1} + v_{K-1} v_K \\
\zeta_2 &= v_1 v_3 + v_2 v_4 + \cdots + v_{K-2} v_K \\
&\vdots \\
\zeta_{K-1} &= v_1 v_K.
\end{aligned} \tag{22}$$

For the designated values of t, x_t is obtained by weighting y_t and $(K-1)$ values of $y_{t\pm m}$ on either side of y_t. The weights are symmetric. For values of t outside of the indicated range, we can construct a filtering interpretation as well. However, edge effects or end effects are observed as the filter coefficients are no longer symmetric.

Eq. (21) is recognized as a noncausal FIR filter, sometimes referred to as an noncausal or non-recursive filter [36]. Since the filter coefficients are symmetric, this is a zero-phase filter as well. It is known that a zero-phase a-casual filter can be obtained by a two-step filtering algorithm [35]. First, filter the data $y_t, t = 1, 2, \ldots, N$ with the FIR filter $v(z^{-1})$ to produce the series $\tilde{w}_t$. Second, filter the series $\tilde{w}_t$ using the FIR filter $\tilde{v}(z^{-1})$, where $\tilde{\boldsymbol{v}} = \boldsymbol{J}\boldsymbol{v}$. This is equivalent to reversing the order of $\tilde{w}_t$ and filtering with $\tilde{\boldsymbol{v}}$, and then reversing the order of the resulting series. In both cases the filtering algorithm uses $y_t = 0$ when $t \le 0$ and $\tilde{w}_t = 0$ when $t > N$. Once the double-filtered series is obtained, it is multiplied by the diagonal weighting matrix $\boldsymbol{D}$. A very close approximation to any of the individuals via rank-1 approximations, $\boldsymbol{x}_i$, is obtained by using the MATLAB® command `filtfilt(`$\boldsymbol{v}$`, 1, y)` and then multiplying the result by $\frac{1}{K}$. Except for a short transient at the beginning and at the end of the reconstructed series, the results coincide with those obtained by diagonal averaging. There are other choices for initial conditions [35] that may be advantageous to reduce edge effect transients. However, due to the length of

$$\boldsymbol{A_1} = \begin{pmatrix} \frac{1}{2}(\boldsymbol{y}_1 + \boldsymbol{y}_K) & \frac{1}{2}(\boldsymbol{y}_2 + \boldsymbol{y}_{K-1}) & \cdots & \frac{1}{2}\left(\boldsymbol{y}_{\left[\frac{K}{2}\right]} + \boldsymbol{y}_{\left[\frac{K}{2}\right]+2}\right) & \boldsymbol{y}_{\left[\frac{K}{2}\right]+1} \end{pmatrix}. \tag{19}$$

Box I.

$$\boldsymbol{A_2} = \begin{pmatrix} \frac{1}{2}(\boldsymbol{y}_1 - \boldsymbol{y}_K) & \frac{1}{2}(\boldsymbol{y}_2 - \boldsymbol{y}_{K-1}) & \cdots & \frac{1}{2}\left(\boldsymbol{y}_{\left[\frac{K}{2}\right]} - \boldsymbol{y}_{\left[\frac{K}{2}\right]+2}\right) & \boldsymbol{0} \end{pmatrix}. \tag{20}$$

Box II.

series and small K value typically encountered in SSA analysis, edge effects are most often small.

The results in this section apply only to signals reconstructed from rank-1 approximations, say, $\boldsymbol{X}_i$. The grouping of several rank-1 reconstructions before averaging is equivalent to calculating the individual averaging operators and then grouping the resulting reconstructions. Consequently, if a rank-p approximation is desired, then p of these filters are arranged in a parallel configuration and the results are summed [22]. A similar idea was also developed in [37].

4. Spectral interpretation of SSA

4.1. Spectral interpretation of latent variables

The spectrum of the filtered series in Eq. (15) is given by

$$S_{\boldsymbol{w}}(f) \simeq |v(\mathrm{e}^{-j2\pi f})|^2 \cdot S(f) \tag{23}$$

where f is the normalized frequency, $0 \le f \le 0.5$, $S(f)$ is the spectrum of y_t, and $|\cdot|$ denotes the magnitude of the quantity '·'. The approximation arises from the assumption that the spectrum of $y_t, t = 1, 2, \ldots, N$, is the same as the spectrum of $y_t, t = K, K+1, \ldots, N$, i.e., edge or end effects have been neglected.

4.2. Spectral interpretations using the Toeplitz approximation

The interesting spectral features of the filtered signals arise from the structured nature of the eigenfilters.

Using the Toeplitz approximation, the eigenfilters are either palindromic or antipalindromic. Any eigenfilter $v(z^{-1})$ can be factorized as [32]

$$v(z^{-1}) = c(z^{-1}-1)^{k_1}(z^{-1}+1)^{k_2}\prod_{i=1}^{k_3}(z^{-2} - 2\cos(\omega_i)z^{-1} + 1) \times \prod_{i=1}^{k_4} e_4(\zeta_i, z^{-1}) \prod_{i=1}^{k_5} e_5(\tau_i, z^{-1}). \tag{24}$$

The term $(z^{-2} - 2\cos(\omega_i)z^{-1} + 1)$ accounts for the complex roots (except ± 1) of unit magnitude, $e_4(\cdot)$ accounts for all real roots except those at ± 1, and $e_5(\cdot)$ accounts for the complex roots, which are neither purely real nor purely imaginary. $\{c, \zeta_i, \omega_i\} \in \mathbb{R}$, $\{\tau_i\} \in \mathbb{C}$, and $K = k_1 + k_2 + 2k_3 + 2k_4 + 4k_5$.

The limiting cases for the spectrum of the filtered signal $\boldsymbol{w}$, at $f = 0$ and $f = 0.5$, are

$$\begin{aligned} \lim_{f\to 0} S_{\boldsymbol{w}}(f) &\simeq \lim_{f\to 0} |v(\mathrm{e}^{-j2\pi f})|^2 \cdot S(f) \\ &= \left| c0^{k_1}2^{k_2}\prod_{i=1}^{k_3} 2(1-\cos(\omega_i)) \prod_{i=1}^{k_4} e_4 \times (\Delta_i, 1)\prod_{i=1}^{k_5} e_5(\tau_i, 1)\right|^2 \cdot S(0) \\ &= 0, \quad k_1 > 0 \end{aligned} \tag{25}$$

Table 3
The frequency characteristics for eigenfilters of Toeplitz matrix.

Type	Order $(K-1)$	$\lim_{f\to 0} \lvert v(\mathrm{e}^{-j2\pi f})\rvert^2$	$\lim_{f\to 0.5} \lvert v(\mathrm{e}^{-j2\pi f})\rvert^2$
Antipalindrome	Odd	0	–
	Even	0	0
Palindrome	Odd	–	0
	Even	–	–

$$\begin{aligned} \lim_{f\to 0.5} S_{\boldsymbol{w}}(f) &\simeq \lim_{f\to 0.5} |v(\mathrm{e}^{-j2\pi f})|^2 \cdot S(f) \\ &= \left| c(-2)^{k_1}0^{k_2}\prod_{i=1}^{k_3} 2(1+\cos(\omega_i)) \prod_{i=1}^{k_4} e_4 \times (\Delta_i, -1)\prod_{i=1}^{k_5} e_5(\tau_i, -1)\right|^2 \cdot S(0.5) \\ &= 0, \quad k_2 > 0. \end{aligned} \tag{26}$$

Using the results in Property 5 and Table 2, the low and high frequency characteristics of the eigenfilters are shown in Table 3. The frequency characteristics are much different from typical digital filters, and are more reminiscent of the filtering characteristics of Slepian functions [38,39].

When $v(z^{-1})$ corresponds to the minimum or maximum eigenvalue, all roots are on the unit circle [17,33]. Consequently, $|v(\mathrm{e}^{-2j\pi f})|$ will be zero at most $(K-1)$ values of f in the interval $0 \le f \le 0.5$, resulting in complete attenuation of $S_{\boldsymbol{w}}(f)$ at these frequencies. We also note that an antipalindromic eigenfilter can always be written as $v(z^{-1}) = (z^{-1}-1)^{k_1}\overline{v}(z^{-1})$, where k_1 is odd and $\overline{v}(z^{-1})$ is a palindromic eigenfilter [32]. Thus, an antipalindromic filter is always equivalent to palindromic filtering of the differenced variable $(z^{-1}-1)^{k_1}y_t$.

4.3. Spectral interpretation of the reconstructed series

As shown in Section 3, a series produced by the diagonal-averaging approach is fundamentally different from the latent variable. The spectral characteristic of a new reconstructed series $\boldsymbol{x}$ follows immediately from Eq. (21).

$$S_{\boldsymbol{x}}(f) \simeq \frac{1}{K^2}|v(\mathrm{e}^{-j2\pi f})|^4 \cdot S(f), \quad 0 \le f \le 0.5. \tag{27}$$

The approximation again arises from the end or edge effects, which are expected to be small when $L \gg K$. The spectral properties of this associated filter follow immediately from the previous discussion.

5. Examples

5.1. Example 1: harmonic series with two real sinusoids

In this section, we consider the following process

$$y_t = \sum_{k=1}^{2} \alpha_k \sin(2\pi f_k t) + \xi_t \tag{28}$$

where $\alpha_k = (4, 2)^T$, $f_k = (0.1, 0.4)^T$, and $\xi_t \sim \mathcal{N}(0, 1)$, ξ_t is

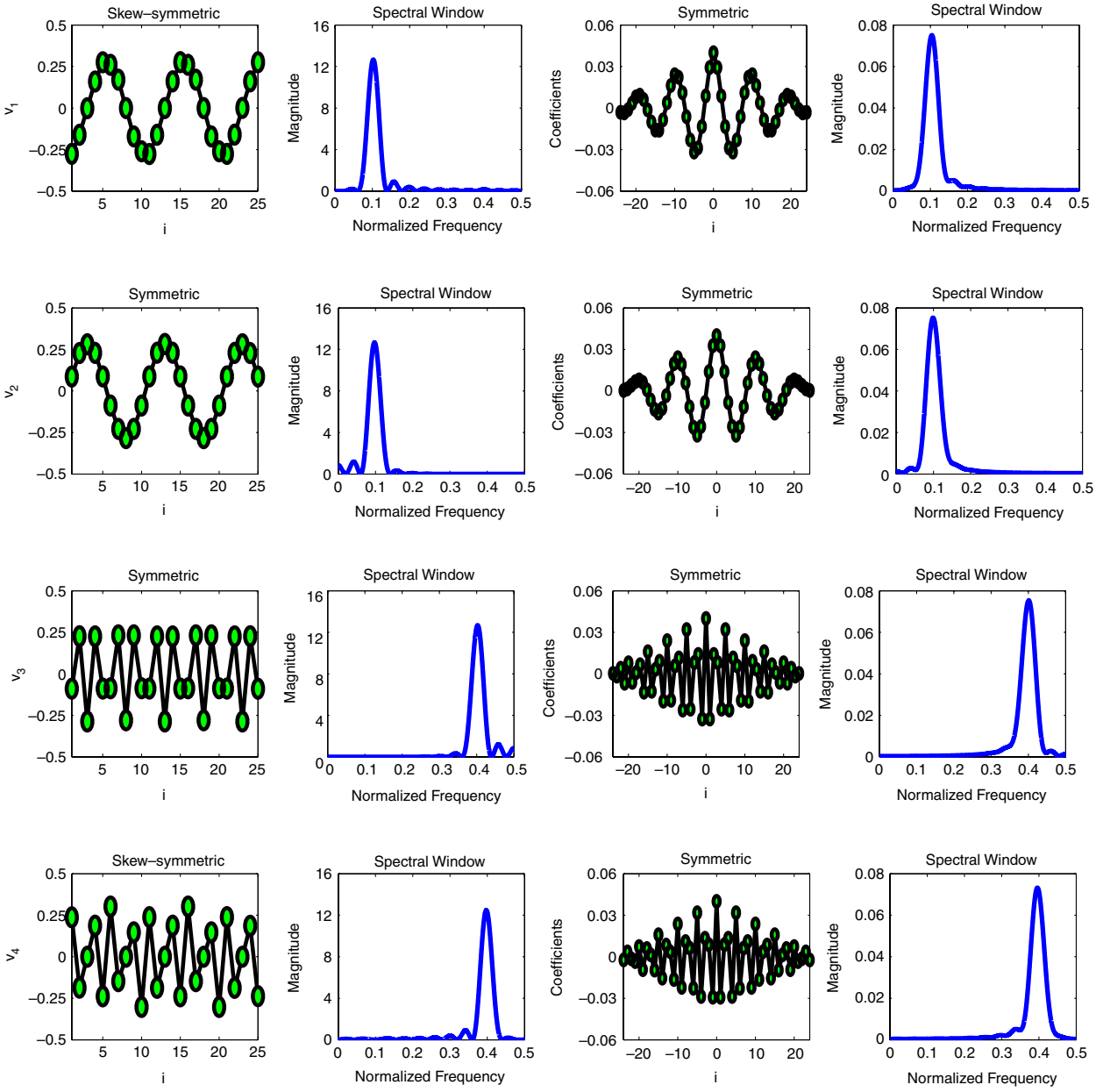

Fig. 1. Filtering and spectral interpretations of example 1. (a) First four eigenvectors (first column); (b) Magnitude of eigenfilter spectrum (second column); (c) Convolution filter coefficients (third column); (d) Magnitude of convolution filter spectrum (fourth column).

normally distributed with mean 0 and variance 1. The simulated data length, N, is 1024. Both the signal and the noise are mean corrected for purposes of analysis. The signal-to-noise ratio (SNR) is 10.

5.1.1. Scree plot and eigenvector analysis

In this example, we choose $K = 25$. The scree plot (not shown) gives four significant eigenvalues, grouped into two pairs. One might anticipate that these two groups of eigenvalues arise from the presence of the two harmonics in the data that correspond to frequencies 0.1 and 0.4. The presence of additive noise produces a large number of much smaller eigenvalues.

We use the Toeplitz approximation $\boldsymbol{A}^T\boldsymbol{A} \simeq \boldsymbol{LC}$ to calculate the SVD. This is a reasonable assumption, as indicated by the Frobenius norm ratio.

$$\frac{\|\boldsymbol{A}^T\boldsymbol{A} - \boldsymbol{LC}\|_F}{\|\boldsymbol{A}^T\boldsymbol{A}\|_F} = \frac{389.7 - 388.2}{388.2} = 0.031. \tag{29}$$

The first four eigenvectors are shown in the first column of Fig. 1. As discussed in Section 3, all the eigenvectors are either symmetric or skew-symmetric. In this example, there are 13 symmetric eigenvectors, and 12 skew-symmetric eigenvectors.

5.1.2. Eigenfilter analysis

From Property 5, the eigenfilters obtained from the first four eigenvectors above are either palindromic or antipalindromic. The magnitude of the associated spectral windows of these eigenfilters is shown in the second column in Fig. 1. The spectral windows show strong peaks at the harmonic frequencies, indicating that the filtering algorithm behaves similar to a notch filter [36].

The roots for these eigenfilters are shown in Fig. 2. (The first panel in Fig. 2 corresponds to the largest eigenvalue.) The number of roots located at $z^{-1} = \pm 1$ for each eigenfilter is noted on the top of each subfigure. The roots at ± 1 follow the properties shown in

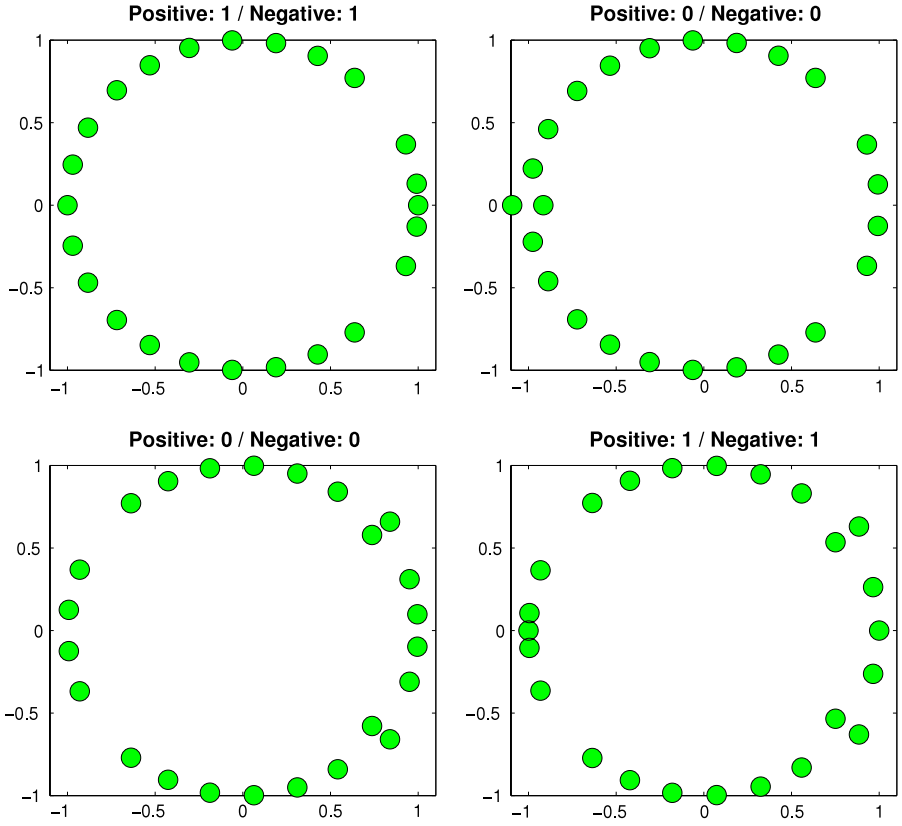

Fig. 2. Roots for the eigenfilters of example 1. The number of roots located at $z^{-1} = \pm 1$ is shown on the top of each panel.

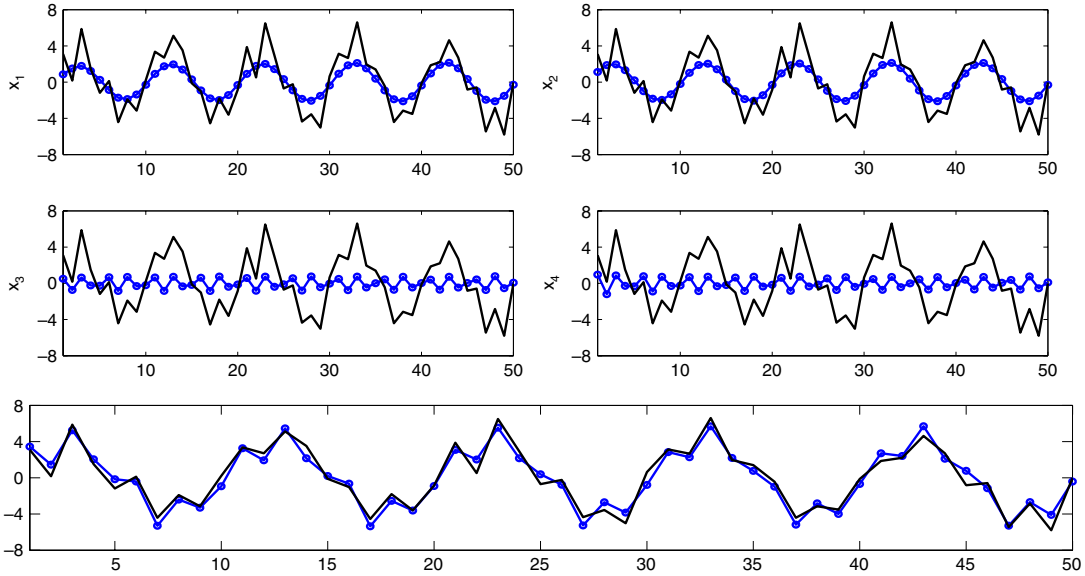

Fig. 3. First four RCs and the grouped series (dotted line) versus original series (solid line) of example 1.

Table 2. The eigenvalues are unique, so the zeros of eigenfilters associated with the smallest and largest eigenvalues all lie on the unit circle.

5.1.3. Convolution filter analysis

The third column in Fig. 1 depicts the convolution filter coefficients. These are all zero-phase filters due to the symmetry of the filter coefficients. The magnitude of the spectral windows of corresponding convolution filters is shown in the fourth column of this figure. The peaks in these spectral plots correspond exactly to the significant frequencies in the signal, i.e., $f = 0.1$ and 0.4. The properties in Table 3 also hold.

5.1.4. Reconstructed components (RCs)

The top four panels in Fig. 3 show the first four RCs obtained by diagonal averaging. The original data is also included in each of these plots. Several observations can be made: (i) the RCs are paired, and each pair has almost the same pattern, and (ii) the first two RCs are much larger than the second two RCs. This is expected as the first two RCs correspond to the harmonic whose

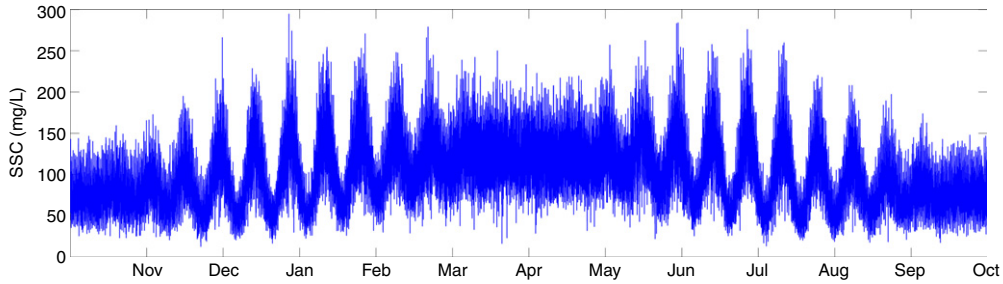

Fig. 4. Synthetic SSC time series.

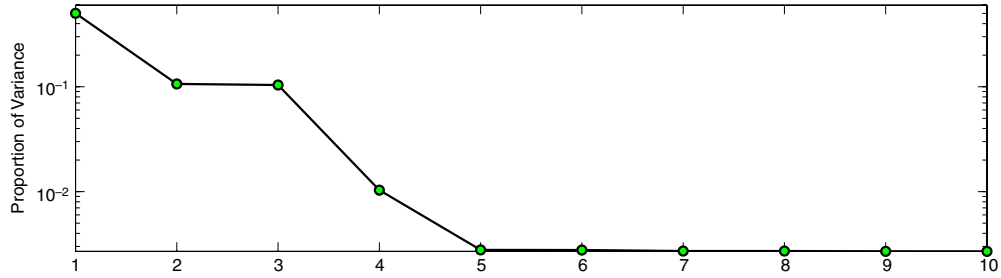

Fig. 5. Scree plot of synthetic SSC series.

frequency is 0.1 and whose power magnitude is four times that of the second harmonic (see Eq. (28)). The last panel in Fig. 3 shows the grouped reconstructed series from the first four RCs. The group reconstructed series closely matches the original data. There is no discernible phase lag, which is to be expected.

5.2. Example 2: synthetic SSC data

As an example, we consider a synthetic suspended-sediment concentration (SSC) series shown in Fig. 4 and analyzed by Schoellhamer [9]. A 15 min SSC time series with mean 100 mg/L was generated using Eqs. (6) and (7) in [9].

$$y(t) = 0.2\epsilon(t)c_s(t) + c_s(t) \tag{30}$$

and

$$c_s(t) = 100 - 25\cos\omega_s t + 25(1-\cos 2\omega_s t)\sin\omega_{sn} t + 25(1+0.25(1-\cos 2\omega_s t)\sin\omega_{sn} t)\sin\omega_a t \tag{31}$$

where ϵ_t is normally distributed random variate with zero mean and unit variance. The seasonal angular frequency $\omega_s = 2\pi/365$ day^{-1}, the spring/neap angular frequency $\omega_{sn} = 2\pi/14$ day^{-1} and the advection angular frequency $\omega_a = 2\pi/(12.5/24)$ day^{-1}.

Eq. (31) was simulated for one water year, giving 35,040 'observations' for analysis. Prior to analysis the data was mean corrected.

5.2.1. Scree plot and eigenvector analysis

In this example, we choose window length $K = 121$. We note that Schoellhamer [9] used $K = 120$. Our analysis is based on the Toeplitz matrix. This provides a very good approximation to $\boldsymbol{A}^T\boldsymbol{A}$ as indicated by the Frobenius norm ratio which has the value 0.002.

The scree plot for the eigenvalues, Fig. 5, has been normalized by the sum of the eigenvalues since the eigenvalues are very large. Note the log scale on the vertical axis. The first three eigenvalues are an order of magnitude larger than the remaining ones. The presence of many small eigenvalues suggests that the data contains aperiodic or random components. Only one group of paired eigenvalues is evident in Fig. 5. One might anticipate three groups of paired eigenvalues, given the structure of the model. An explanation for this behavior is given in the next subsection.

By using the Toeplitz approximation, 61 symmetric and 60 skew-symmetric eigenvectors are obtained. The first column of Fig. 6 shows the first three eigenvectors.

5.2.2. Eigenfilter analysis

The magnitude of the associated spectral windows of these eigenfilters is shown in the second column in Fig. 6. The spectral window corresponding to the largest eigenvalue has the characteristics of a low-pass filter. The second and third eigenfilters correspond to a **notch filter** with normalized frequency of 0.02. This frequency corresponds to the advection angular frequency $\omega_a = 2\pi/(12.5/24)$ day^{-1}. Given the data and model, we may expect three groups of paired eigenvalues. However, by only simulating one year's data, the subtidal (annual) cycle shows up as a low frequency component. Thus, this effect is captured in the first eigenfilter. However, this eigenfilter also smooths out the effect of the fortnight component, which appears at the normalized frequency 7.44×10^{-4}. Advanced spectral methods such as Thompson's multi-taper method [38,39] readily separate the fortnight/advection components. Additional insights into the spectrum are often obtained by using several spectral methods [40,41].

The roots of the eigenfilters follow the same properties in Table 2 and example 1. Additionally, all the roots of eigenfilters related to smallest and largest eigenvalues are located on the unit circle. Due to similarity, the root plots are not shown.

5.2.3. Convolution filter analysis

The convolution filter coefficients are shown in the third column of Fig. 6 and the corresponding spectral characteristics of these filters are shown in the fourth column of this figure. The convolution filter corresponding to the largest eigenvalue has a distinctively triangular shape and acts as a low-pass filter. The second and third convolution filters have their power concentrated at a normalized frequency of 0.02.

5.2.4. Reconstructed components (RCs)

The first three RCs are plotted in the last three panels of Fig. 7. Individually they account for 48.7%, 5.1%, and 5.0% of the variation in the data. (The data variance is 1546.7.) Table 4 confirms that the RCs are not orthogonal.

The first RC is a very smooth signal, reflecting that it is obtained by a low-pass filtering of the data. By comparing the patterns of the other two RCs, it is clear that the identification of the harmonic component has been done correctly, as the convolution filter acts like a notch filter.

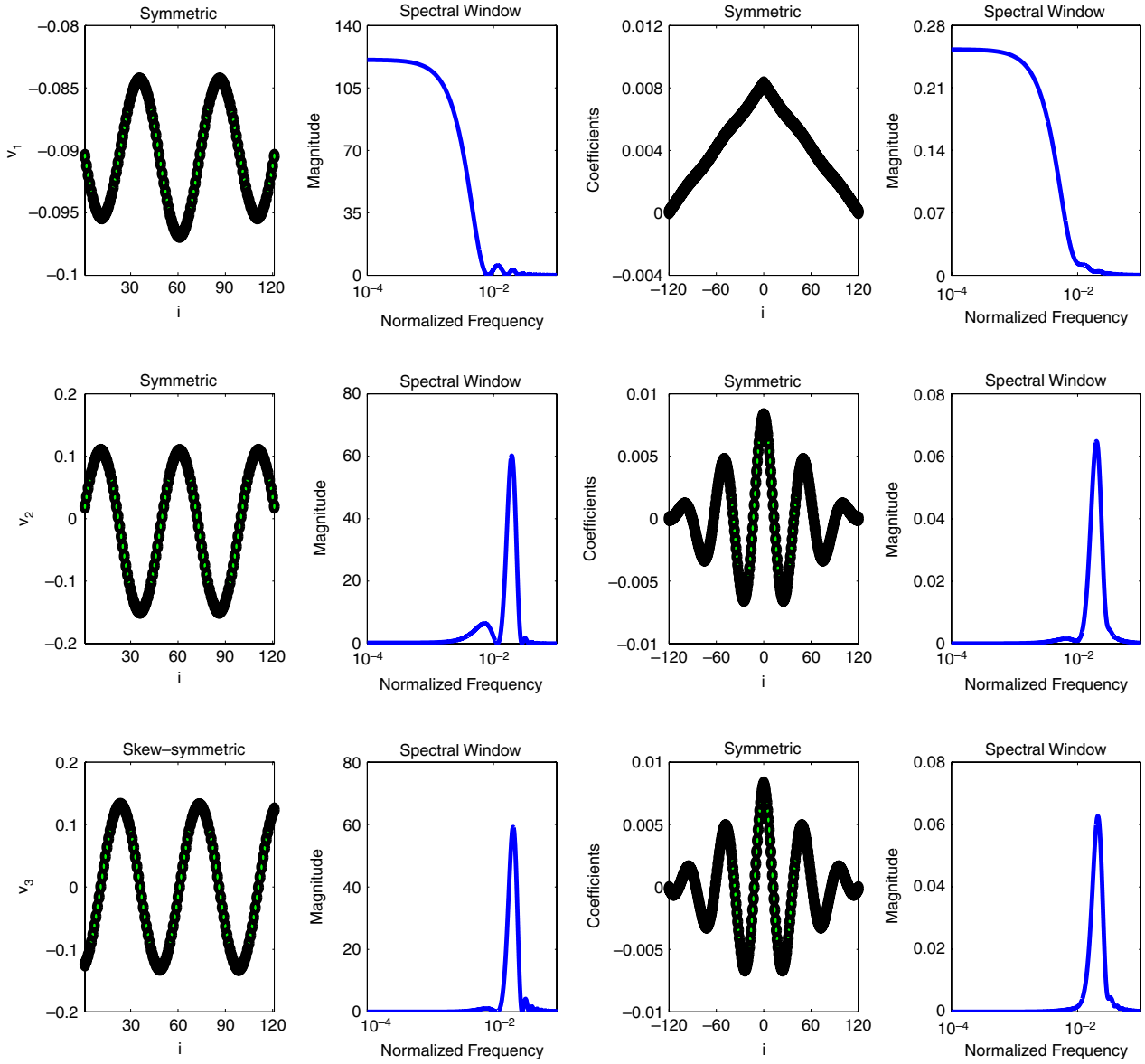

Fig. 6. Filtering and spectral interpretations of synthetic SSC series. (a) First three eigenvectors (first column); (b) Magnitude of eigenfilter spectrum (second column); (c) Convolution filter coefficients (third column); (d) Magnitude of convolution filter spectrum (fourth column).

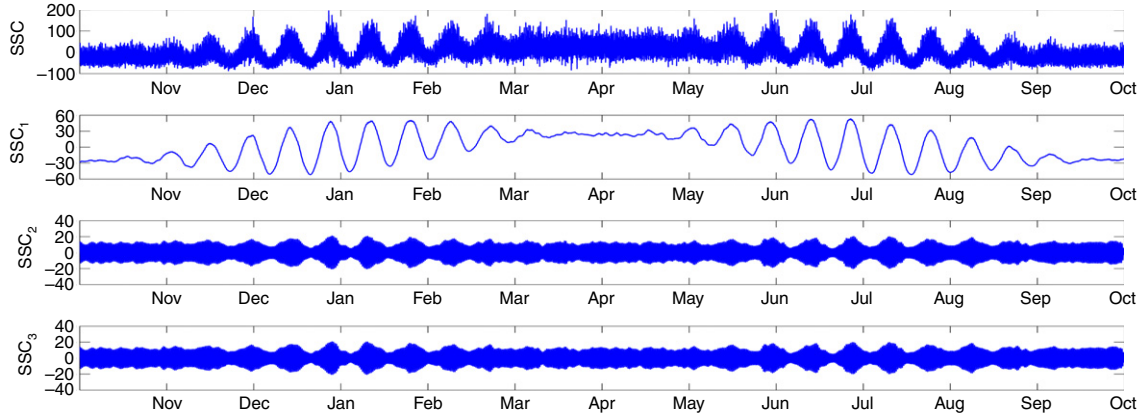

Fig. 7. Synthetic SSC series along with the first three RCs.

Table 4
Variance summary of first three components.

a	$\frac{\lambda_i}{\sum_{i=1}^{K}\lambda_i}$	$\mathrm{var}(\boldsymbol{x}_i)$	$\sum_{i=1}^{a}\mathrm{var}(\boldsymbol{x}_i)$	$\mathrm{var}\left(\sum_{i=1}^{a}\boldsymbol{x}_i\right)$
1	0.5011	745.1	745.1	745.1
2	0.1064	81.2	826.3	838.1
3	0.1039	79.2	905.5	1086.1

6. Conclusion and discussion

Singular Spectrum Analysis is a flexible and useful method for time-series analysis. The primary contributions of this paper have been to provide additional insights into the filtering and spectral characteristics of SSA technology and the enhancements that arise by using diagonal averaging. These new results are derived from the properties of symmetric Toeplitz matrices and the properties of the resulting eigenfilters and convolution filters. Filtering and spectral interpretations for the reconstructed series from diagonal averaging were derived. The symmetric and skew-symmetric behavior of the eigenfilters was exploited to derive a number of these properties. It was shown that the reconstructed series could be interpreted as zero-phase filtered responses, obtained by a particular implementation of forward and reverse filtering of the original data. It was also shown that whereas the latent variables are orthogonal, the reconstructed series are not orthogonal. The results in this paper should enable a more thorough comparison of SSA with other filtering methods.

Multichannel extensions of SSA (MSSA) have been proposed [42–44]. MSSA produces data-adaptive filters that can be used separate patterns both in time and space. It is necessary to construct a 'grand' block matrix, a multichannel equivalent to $\boldsymbol{A}^T\boldsymbol{A}/L$. This matrix also has a block Toeplitz approximation. This approximation gives a symmetric, but not persymmetric grand matrix, although every sub-block matrix is a persymmetric matrix. Exploitation of the properties of these highly structured matrices to ascertain filtering and spectral properties, in a manner similar to that employed in this paper, should be possible.

References

[1] G.C. Castagnoli, C. Taricco, S. Alessio, Isotopic record in a marine shallow-water core: imprint of solar centennial cycles in the past 2 millennia, Adv. Space Res. 35 (2005) 504–508.
[2] R. Vautard, M. Ghil, Singular spectrum analysis in nonlinear dynamics, with applications to paleoclimatic time series, Physica D 35 (1989) 395–424.
[3] R. Vautard, P. Yiou, M. Ghil, Singular-spectrum analysis: a toolkit for short, noisy chaotic signals, Physica D 58 (1992) 95–126.
[4] G.T. Jemwa, C. Aldrich, Classification of process dynamics with Monte Carlo singular spectrum analysis, Comput. Chem. Eng. 30 (2006) 816–831.
[5] G. Tzagkarakis, M. Papadopouli, T. Panagiotis, Singular spectrum analysis of traffic workload in a large-scale wireless lan, in: Proceedings of the 10th ACM Symposium, 2007, pp. 99–108.
[6] M. Papadopouli, G. Tzagkarakis, T. Panagiotis, Trend forecasting based on singular spectrum analysis of traffic workload in a large-scale wireless lan, Perform. Eval. 66 (2009) 173–190.
[7] C. Penland, M. Ghil, K.M. Weickmann, Adaptive filtering and maximum entropy spectra with application to changes in atmospheric angular momentum, J. Geophys. Res. Atmos. 96 (1991) 22659–22671.
[8] SSA-MTM group, mostly, UCLA, SSA-MTM toolkit for spectral analysis. http://www.atmos.ucla.edu/tcd/ssa/.
[9] D.H. Schoellhamer, Singular spectrum analysis for time series with missing data, Geophys. Res. Lett. 28 (2001) 3187–3190.
[10] P. Yiou, D. Sornette, M. Ghil, Data-adaptive wavelets and multi-scale singular-spectrum analysis, Physica D 142 (2000) 254–290.
[11] E.R. Pike, J.G. McWhirter, M. Bertero, C.D. Mol, Generalized information theory for inverse problems in signal-processing, Commun. Radar Signal Process. IEE Proc. F 131 (1984) 660–667.
[12] D.S. Broomhead, G.P. King, Extracting qualitative dynamics from experimental data, Physica D 20 (1986) 217–236.
[13] N. Golyandina, V. Nekrutkin, A. Zhigljavsky, Analysis of Time Series Structure: SSA and Related Techniques, Chapman & Hall/CRC, 2001.
[14] H. Hassani, Singular spectrum analysis: methodology and comparison, J. Data Sci. 5 (2007) 239–257.
[15] A. Cantoni, P. Butler, Eigenvalues and eigenvectors of symmetric centrosymmetric matrices, Linear Algebra Appl. 13 (1976) 275–288.
[16] A. Cantoni, P. Butler, Properties of the eigenvectors of persymmetric matrices with applications to communication theory, IEEE Trans. Commun. COM-24 (1976) 804–809.
[17] J. Makhoul, On the eigenvectors of symmetric Toeplitz matrices, in: Proceedings of the Acoustics, Speech, and Signal Processing, vol. 29, 1981, pp. 868–872.
[18] R.B. Catell, Scree test for the number of factors, Multivariate Behav. Res. 1 (1966) 245–276.
[19] J.C. Hayton, D.G. Allen, V. Scarpello, Factor retention decisions in exploratory factor analysis: a tutorial on parallel analysis, Organ. Res. 7 (2004) 191–205.
[20] M. Ghil, M.R. Allen, M.D. Dettinger, et al., Advanced spectral methods for climatic time series, Rev. Geophys. 40 (2002) 1003.
[21] G.H. Golub, C.F. VanLoan, Matrix Computations, 3rd ed., John Hopkins University Press, Baltimore, 1996.
[22] P.C. Hansen, S.H. Jensen, FIR filter representations of reduced-rank noise reduction, IEEE Trans. Signal Process. 46 (1998) 1737–1741.
[23] R. Kumaresan, D. Tufts, Estimating the parameters of exponentially damped sinusoids and pole-zero modeling in noise, IEEE Trans. Acoust. Speech Signal Process. 30 (1982) 833–840.
[24] Y. Li, K.J.R. Liu, J. Razavilar, A parameter estimation scheme for damped sinusoidal signals based on low-rank hankel approximation, IEEE Trans. Signal Process. 45 (1997) 481–486.
[25] J. Razavilar, Y. Li, K.J.R. Liu, A structured low-rank matrix pencil for spectral estimation and system identification, Signal Process. 65 (1998) 363–372.
[26] J. Razavilar, Y. Li, K.J.R. Liu, Spectral estimation based on structured low rank matrix pencil, in: Proc. IEEE Int. Conf. Acoust. Speech Signal Processing, 1996, pp. 2503–2506.
[27] M.T. Chu, R.B. Funderlic, R.J. Plemmons, Structured low rank approximation, Linear Algebra Appl. 366 (2003) 157–172.
[28] J.A. Cadzow, Signal enhancement-a composite property mapping algorithm, IEEE Trans. Acoust. Speech Signal Process. 36 (1988) 49–62.
[29] B.D. Moor, Total least squares for affinely structured matrices and the noisy realization problem, IEEE Trans. Signal Process. 42 (1994) 3104–3113.
[30] I. Markovsky, J.C. Willems, S.V. Huffel, B.D. Moor, R. Pintelon, Application of structured total least squares for system identification and model reduction, IEEE Trans. Autom. Control 50 (2005) 1490–1500.
[31] L.L. Scharf, The SVD and reduced rank signal processing, Signal Process. 25 (1991) 113–133.
[32] I. Markovsky, S. Rao, Palindromic polynomials, time-reversible systems, and conserved quantities, in: Control and Automation, 2008 16th Mediterranean Conference, June 2008, pp. 125–130.
[33] E.A. Robinson, Statistical Detection and Estimation, Halfner, 1967.
[34] S.S. Reddi, Eigenvector properties of Toeplitz matrices and their application to spectral anaysis of time series, Signal Process. 7 (1984) 45–56.
[35] J. Kormylo, V. Jain, Two-pass recursive digital filter with zero phase shift, in: Proceedings of the Acoustics, Speech, and Signal Processing, vol. AS22, 1974, pp. 384–387.
[36] C.S. Lindquist, Adaptive & Digital Signal Processing with Digital Filtering Applications, Stewart & Sons, 1989.
[37] I. Dologlou, G. Carayannis, Physical interpretation of signal reconstruction from reduced rank matrices, IEEE Trans. Signal Process. 39 (1991) 1681–1682.
[38] D.J. Thomson, Spectrum estimation and harmonic analysis, Proc. IEEE 70 (1982) 1055–1096.
[39] D.B. Percival, A.T. Walden, Spectral Analysis for Physical Applications: Multitaper and Conventional Univariate Techniques, Cambridge University Press, 1993.
[40] P. Yiou, B. Baert, M.F. Loutre, Spectral analysis of climate data, Surv. Geophys. 17 (1996) 619–663.
[41] M. Ghil, C. Taricco, Advanced spectral analysis methods, in: G. Cini Castagnoli, A. Provenzale (Eds.), Past and Present Variability of the Solar-Terrestrial System: Measurement, Data Analysis and Theoretical Models, Societa Italiana Di Fisica, Bologna, IOS Press, Amsterdam, 1997, pp. 137–159.
[42] G. Plaut, R. Vautard, Spells of low-frequency oscillations and weather regimes in the northern hemisphere, J. Atmospheric Sci. 51 (1994) 210–236.
[43] L.V. Zotova, C.K. Shumb, Multichannel singular spectrum analysis of the gravity field data from grace satellites, AIP Conf. Proc. 1206 (2010) 473–479.
[44] S. Raynaud, P. Yiou, R. Kleeman, S. Speich, Using MSSA to determine explicitly the oscillatory dynamics of weakly nonlinear climate systems, Nonlinear Processes Geophys. 12 (2005) 807–815.